J Mater Sci (2011) 46:3611–3621
DOI 10.1007/s10853-011-5277-2

Preparation and chemical reduction of laurylamine-intercalated graphite oxide

Yanyun Wang · Linsheng Xie · Jin Sha · Yulu Ma · Jingjie Han · Shumei Dong · Hu Liu · Cheng Fang · Shuyun Gong · Zhangqi Wu

Received: 11 November 2010 / Accepted: 12 January 2011 / Published online: 5 February 2011

Abstract Laurylamine-intercalated graphite oxide (GO) is prepared by ultrasonic in the presence of a small amount of hexane and then chemically reduced by hydrazine. The interlayer spacing of laurylamine-intercalated GO reaches a maximum when the molar ratio of laurylamine and GO is 1.384. Three types of laurylamine in GO are identified in the intercalated compounds: hydrogen-bonded neutral amines, hydrogen-bonded protonated amines, and ionically bound protonated amines. Modified graphene colloidal suspension is obtained by chemical reduction of laurylamine-intercalated GO in dimethyl formamide (DMF). Furthermore, a possible chemical reduction mechanism is put forward to explain the hydrazine reduction process.

Introduction

Graphite oxide (GO) is an oxygen-rich derivative of graphite. The large quantities of oxygen exist in the form of epoxy, hydroxyl, and carboxyl groups [1, 2]. Due to the layer structure and oxygen functional groups, the GO is hydrophilic and easily hybridize with other species [3]. Various modified GO are synthesized by the reaction of exfoliated GO layers and polymers, polar molecules, alkyltrimethylammonium ions, or surfactant [4–9]. The modified GO can produce homogeneous colloidal suspensions in various solvents and influence the properties of GO. The abilities of modified GO to recognize aromatic molecules [10], control aggregation state and orientation of organic dyes [11], application as cathode-active materials candidates for lithium batteries [12] have been reported.

The modified GO is known as modified graphene oxide when it forms homogeneous colloidal suspensions in various solvents. One of the most important reactions of graphene oxide is its reduction with hydrazine in the solvents which provides a promising route to achieve mass production of graphene platelets.

The graphene is atomically thin two-dimensional sheet of carbon. It has attracted considerable attention as promising components in applications such as energy-storage materials [13], "paper-like" materials [14], polymer composites [15, 16], and mechanical resonators [17], given the predicted excellent in-plane mechanical, structural, thermal, and electrical properties [18–21]. In practice, reduction of well-dispersed GO nanoplatelets results in a gradual decrease in their hydrophilic character, which eventually leads to their irreversible agglomeration and precipitation [22]. However, many applications inevitably depend on the dispersion ability of graphene in the materials. The first step for application in the materials often involves in obtaining well-dispersed mixture of graphene and materials in some kind of solvents. We have proved that alkylamine-intercalated GO can be well dispersed in dimethyl formamide (DMF), forming stable colloidal suspensions even after reduced by hydrazine.

There are some reports about alkylamine-intercalated GO [23–25], but seldom mention the chemical reduction of alkylamine-intercalated GO. In this study, we investigate the preparation of laurylamine-intercalated GO and characterize its reduction in detail.

Y. Wang · L. Xie (✉) · J. Sha · Y. Ma · J. Han · S. Dong · H. Liu · C. Fang · S. Gong · Z. Wu
School of Mechanical and Power Engineering, East China University of Science and Technology, Shanghai 200237, People's Republic of China
e-mail: clxw@ecust.edu.cn

Experimental

Synthesis of GO

Graphite oxide was prepared from natural graphite powder (100 mesh) supplied by Sigma-Aldrich due to the modified Hummers method [26]. About 10 g of graphite powder was added to 230 mL of cooled (0 °C) concentrated H_2SO_4. Then, 30 g of $KMnO_4$ was added gradually with stirring and cooling, keeping the mixture temperature below 5 °C. After that, the mixture was stirred at 5 °C for 30 min and then placed steadily for 96 h. Then the mixture was slowly added into 460 mL of distilled water with stirring and cooling, keeping the mixture temperature below 35 °C. Later, the mixture was heated to 35 °C and kept the temperature for 1 h. After that, the mixture was heated to 98 °C and maintained the temperature for 45 min. Finally, the reaction was terminated by adding 15 mL of 30% H_2O_2 solution. The resulting solution was filtered off, washed repeatedly with 5% HCl solution, followed by excess deionized water, and dried at 60 °C overnight to get the dried GO. The homogeneous GO powder was obtained by ball milling the dried GO in the all-directions planetary mill (Nanjing, QM-QX2) which was performed with rotation speed 300 r/min for 2 h.

Preparations of laurylamine-intercalated GO

Dried GO powder and laurylamine (C_{12}) were mixed followed by a small amount of *n*-hexane to immerse the solid-state mixture. It was observed that C_{12} dissolved quickly in *n*-hexane. Stable dispersion of the laurylamine-intercalated GO [$(C_{12})_xGO$; x:C_{12}/GO molar ratio] was prepared by 15 min ultrasonic exfoliation. The obtained product was placed at room temperature and dried at 60 °C overnight until the hexane fully evaporated. The C_{12}/GO molar ratio changed from 0.198 to 1.780.

Chemical reduction of $(C_{12})_xGO$

Stable dispersion of the $(C_{12})_xGO$ (400 mg) was prepared by ultrasonic exfoliation in DMF (400 mL) for 1 h. Reduction of the dispersed $(C_{12})_xGO$ was carried out with hydrazine (4 mL) at 95 °C for 1 h. The product obtained after reduction was isolated via filtration, washed with deionized water, and dried at 60 °C to remove moisture.

Characterization

The resulting samples were characterized by X-ray diffraction (XRD; Rigaku, D/MAX 2550 VB/PC), infrared spectroscopy (FT-IR; Nicolet, Magna-IR 550, KBr pellets), thermogravimetry (TG; America, SDT Q600), X-ray photoelectron spectroscopy (XPS; PHI, 5000C ESCA), elemental analyzer (Germany, vario EL III), scanning electron microscopy (SEM; JEOL, JSM-6360LV), atomic force microscope (AFM; Veeco, NanoScope IIIa MultiMode). TG measurements were performed under N_2 protection with the temperature increase rate 5 °C/min from room temperature to 800 °C. The method due to Matsuo et al. [24] was adopted to determine the amount of exchangeable acidic groups in the obtained GO by the back titration of sodium hydroxide solution (0.05 mol/L, 50 mL) of GO (100 mg) with hydrochloric acid solution (0.05 mol/L). All the involved chemicals and solvents, including sulfuric acid, potassium permanganate, sodium hydroxide solution, hydrochloric acid solution, laurylamine, DMF, and hydrazine, were purchased from Sinopharm Co. Ltd. and used as received.

Results and discussion

Characterization of GO

Well known as non-stoichiometric compound, the composition of GO is normally measured by elemental analysis and TG analysis [22, 24, 27]. Based on the elemental analysis of carbon and hydrogen, the composition of as prepared GO is $C_8O_{1.84}H_{3.42}{\cdot}0.97H_2O$. The water content is determined from the weight decrease below 200 °C observed by TG analysis [24].

Figure 1 shows the XRD patterns of GO powder. Apart from the diffraction peak at $2\theta = 11.62°$, the diffraction peak of graphite is observed at $2\theta = 26.54°$, indicating the partly oxidization of graphite. It is well known that the oxidation degree of GO depends on many factors, such as the particular oxidants, the graphite size, and the reaction conditions [28, 29]. Although the references about oxidization structure of partly oxidized GO is few, the common

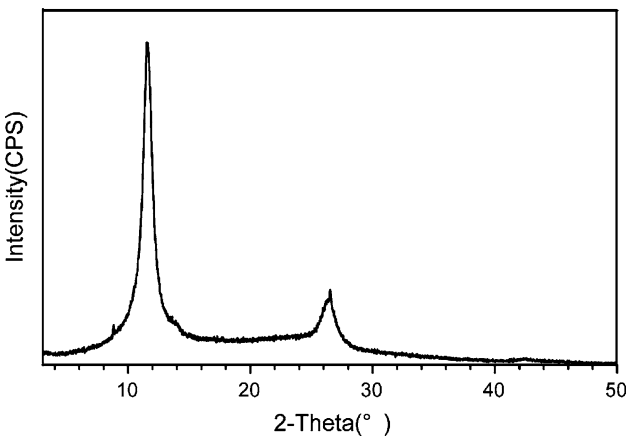

Fig. 1 XRD patterns of GO powder

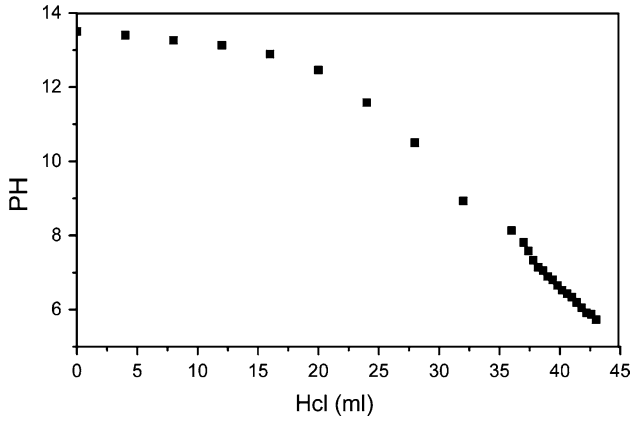

Fig. 2 The pH titration curve of GO dissolved in 0.1 mol/L NaOH aqueous solution toward H^+

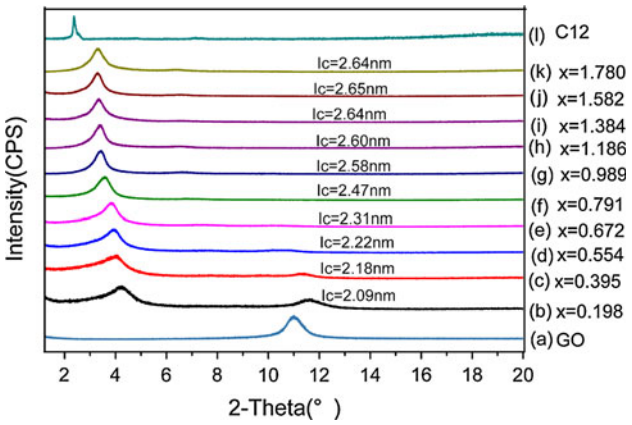

Fig. 3 Small angle XRD of $(C_{12})_xGO$ together with that of C_{12}

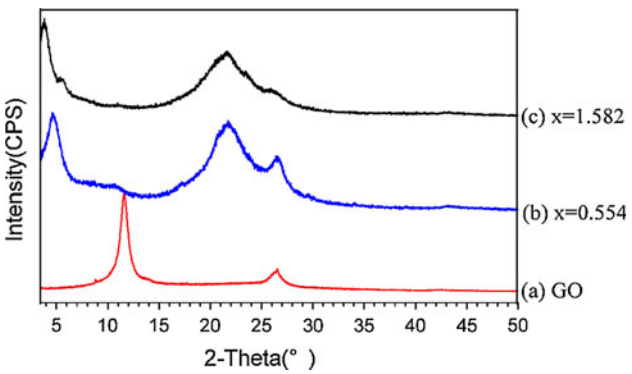

Fig. 4 Wide angle XRD of (*a*) GO, (*b*) $(C_{12})_{0.554}GO$, and (*c*) $(C_{12})_{1.582}GO$

sense about fully oxidized GO concerns more reaction time and more defects, comparing with the partly oxidized GO [30, 31]. On the other hand, partly oxidized structure of obtained GO could be modified by C_{12} and well disperse in DMF even after 1 month steady standing. Therefor, we choose the partly oxidized GO as our starting material to research the modification of GO and its chemical reduction.

The pH titration curve of GO toward H^+ is given in Fig. 2. When 39 mL of H^+ (0.05 mol/L) was added to the well-dispersed colloidal suspension of GO (0.1 g), the pH value of the solution reached 7. Therefore, the total exchange capacity of GO is evaluated as 5.5 mmol/g from the ion-exchange reaction in a 0.1-mol/L HCl solution. This value is comparable to or larger than those reported by Matsuo et al. [24] (3.5 mmol/g) and Cassagneau et al. [32] (3.24–6.04 mmol/g). Szabó et al. [33] pointed out that acidity and cation exchange of GO cannot be characterized by a single value, but depended on the pH and ionic strength. Thus, the cation exchange capacity or acidity of GO determined from titration varies in a wide range. In addition, the titration curve shows a multi-base acid character, suggesting that the synthesized GO contains more than one kind of exchangeable protons.

Characterization of $(C_{12})_xGO$

XRD experiments were conducted to study the effect of the C_{12} molecules on the GO interlayer spacing. Figure 3 shows the small angle XRD of laurylamine-intercalated GO with various C_{12}/GO ratios together with that of C_{12} and GO. For $(C_{12})_xGO$, the diffraction peaks of GO at $2\theta = 11.62°$ and C_{12} at $2\theta = 2.37°$ disappear, and a serials of peaks are observed due to the reaction between GO and various amount of C_{12}. When the C_{12}/GO ratios become larger than 1.186, no obvious change in diffraction of pattern is observed. The saturation amount and I_c value of C_{12} in GO (1.186 mol/GO, $I_c = 2.65$ nm) are smaller than that observed in Matsuo's alkylamine-intercalated GO (1.7 mol/GO, $I_c = 3.65$ nm) [21] with the same alkyl chain length. The differences can be explained by the structure of partly oxidized GO, which will be further discussed in the next paragraph.

As to the peak change situation of GO at $2\theta = 26.54°$ with various C_{12} contents, we researched two types of $(C_{12})_xGO$ ($x = 0.554$, 1.582) which is shown in Fig. 4. The peak of GO at $2\theta = 26.54°$ changes with the different amount of C_{12} in $(C_{12})_xGO$ (Fig. 4b, c). The peak at $2\theta = 26.10°$ ($x = 0.554$) conforms to the peak of graphite and almost disappears when $x = 1.582$. We observed that the pristine GO can readily well disperse in water through ultrasonic exfoliation, while the laurylamine-intercalated GO no longer exfoliates in water. Since the water molecules are removed from the layer of $(C_{12})_xGO$ [24], the influence of humidity level on I_c or 2θ values can be negligible. The new peaks at $2\theta = 21.40°$ ($x = 0.554$) and $2\theta = 21.64°$ ($x = 1.582$) are observed which might due to the structure of partly oxidized GO. The structure is somewhere between graphite and fully oxidized GO. Monolayer of partly oxidized GO consists of two parts: the

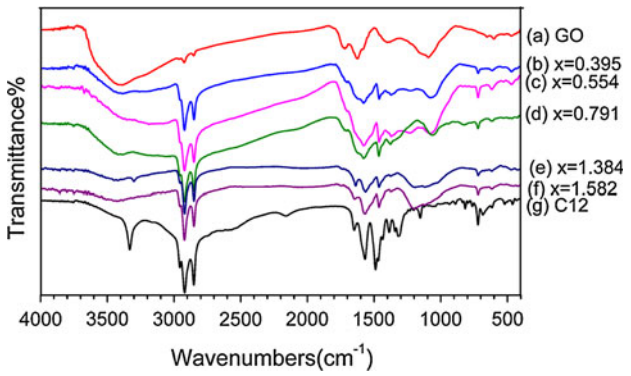

Fig. 5 FT-IR spectra of (*a*) GO, $(C_{12})_xGO$ with various C_{12} contents: (*b*) $x = 0.395$, (*c*) $x = 0.554$, (*d*) $x = 0.791$, (*e*) $x = 1.384$, (*f*) $x = 1.582$, and (*g*) C_{12}

oxidized component reacts with C_{12} and the other un-oxidized component exists in the form of graphitic nanocrystal. The C_{12} intercalation expands the interlayer spacing of oxidized component, and in some way influences the I_c value of un-oxidized component, causing the formation of new peaks at $2\theta = 21.40°$ ($x = 0.554$) and $2\theta = 21.64°$($x = 1.582$). This also explains why the saturation amount and I_c value of C_{12} in GO are smaller than that observed in Matsuo's alkylamine-intercalated GO [21], as shown in Fig. 3.

FT-IR spectra have often been used to probe structural characteristics of graphitic materials, providing useful information on the functional groups. Figure 5 shows FT-IR spectra of GO, C_{12}, and $(C_{12})_xGO$ with various C_{12} contents. In GO, we observe the absorption peak due to –C=O stretching vibrations (1093 cm^{-1}), –C=C stretching vibrations (1628 cm^{-1}), carboxyl groups stretching vibrations (1720 cm^{-1}), and –OH stretching vibrations (3400 cm^{-1}). In all $(C_{12})_xGO$ samples, the absorption peaks due to $–CH_2–$ symmetric and asymmetric stretching vibrations (2956, 2933, 2919, and 2852 cm^{-1}), $–CH_2–$ twist vibrations (1467 cm^{-1}), –C=O stretching vibrations (1093 cm^{-1}), N–H, O–H bending vibrations and –C=C stretching vibrations (1628 cm^{-1}), N–H and –OH stretching vibrations (3400 cm^{-1}) are observed. The absorption peak at 1720 cm^{-1} of GO is observed for $x = 0.395$, 0.554, and 0.791. The C_{12} absorption peaks at 1648 and 1153 cm^{-1} are also observed for $x = 1.384$ and 1.582. The spectrum of $(C_{12})_xGO$ become much similar to C_{12} as the increase of x except for the absence of peaks at 3330, 1488, 2956, and around 800–1100 cm^{-1}. The intensities of the peaks at 3400 and 1628 cm^{-1} decrease from $x = 0.395$ to 1.384, which indicate the decrease of interlayer water content in $(C_{12})_xGO$, confirming to the hydrophobic property of $(C_{12})_xGO$. When $x = 1.582$, the intensities of peaks at 3400 and 1628 cm^{-1} are stronger than those of $x = 1.384$, which are due to the overlap of redundant C_{12} absorption. In addition to the absorption peak at 1628 cm^{-1}, the alkyl ammonium ion also shows a weak absorption peak in the range of 1550–1480 cm^{-1} as expected, which was not be observed by Nethravathi et al. [25] due to either it was too weak or it overlapped with C–H bending absorption at 1470 cm^{-1}. The absorption peak at 1398 cm^{-1} due to hydroxyl groups of acidic character and the absorption peak at 1720 cm^{-1} due to carboxyl groups [34] become much weaker with the increase of x, which indicate that C_{12} molecules have interacted with these groups in GO. The peaks at 1567 and 1648 cm^{-1} are derived of amino groups of C_{12}, though the later may be partly overlapped with that of adsorbed water in GO at 1628 cm^{-1}.These are assigned to the formation of hydrogen bonded of NH_2 [35] in $(C_{12})_xGO$. For $x = 0.395$, 0.554, and 0.791, a weak peak at 1525 cm^{-1} is also expected to be observed, which can be ascribed to the formation of symmetric or asymmetric deformation band of NH_3^+ [24], do not occur in our spectra due to its so weak intensity. The absorption peak at 1093 cm^{-1} due to ether group is almost unchanged along with the increase of C_{12} molecules in GO. For $x = 1.384$ and 1.582, the absorption peak at 1093 cm^{-1}, due to the absorption peak of surplus C_{12}, is broader.

Figure 6 shows the TG curves of $(C_{12})_xGO$, GO, and C_{12}. For $(C_{12})_xGO$, the weight decease is observed below 180 °C due to the elimination of absorbed water or decomposition of C_{12}. Due to the hydrophobic nature of $(C_{12})_xGO$ [36], $(C_{12})_{1.582}GO$ may have a stronger power to exclude water than $(C_{12})_{0.672}GO$ which results in $(C_{12})_{0.672}GO$ decrease dramatically comparing with $(C_{12})_{1.582}GO$. The second weight decrease is observed above 230 °C, which would be mainly because of the elimination of oxygen functionalities from GO layers, leaving residual carbon. The weight is almost constant when the temperature is above 500 °C.

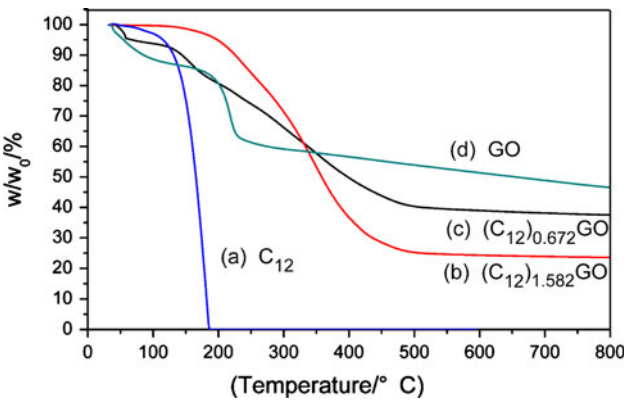

Fig. 6 TG curves of (*a*) C_{12}, (*b*) $(C_{12})_{1.582}GO$, (*c*) $(C_{12})_{0.672}GO$, and (*d*) GO

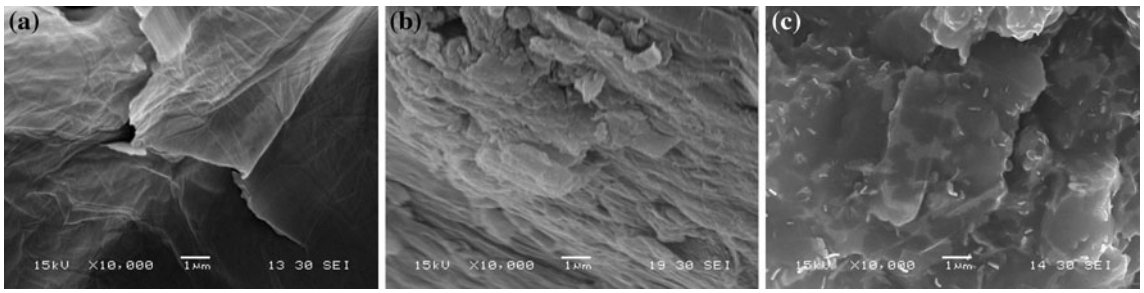

Fig. 7 SEM images of **a** GO, **b** $(C_{12})_{0.395}GO$, and **c** $(C_{12})_{1.582}GO$

Figure 7 shows SEM images of (a) GO, (b) $(C_{12})_{0.395}GO$, and (c) $(C_{12})_{1.582}GO$. As shown in Fig. 7a, GO consists of plate-type crystals reflecting its layered structure. The images of the sample (b) $(C_{12})_{0.395}GO$ which includes lower amines content is similar to that of GO, while (c) $(C_{12})_{1.962}GO$ has a quite different image. The layered structure of GO disappears, and its surface appears to be integrated except for some fissures that might ascribe to the low-melting temperature of C_{12} (melting point: 28 °C): overabundant C_{12} melted and wrapped around the GO, except for the reaction part with GO.

We employed XPS to analyze the samples of $(C_{12})_xGO$ with various C_{12} contents to help us better understand the functional groups information. Figure 8a shows the N_{1s} XPS spectrum of $(C_{12})_{0.554}GO$. The peak which is deconvoluted into two peaks at 399.4 and 400.7 eV indicates different functional groups: the hydrogen-bonded NH_2 (Fig. 10a) and hydrogen-bonded protonated amines (Fig. 10b), respectively [24, 30]. The peak at 400.7 eV is assigned to nitrogen atoms from ammonium group which weakly bond to the GO layer via hydrogen bond [24]. The possible structure is shown in Fig. 10b. For $(C_{12})_{1.780}GO$ (Fig. 8b), the peak is deconvoluted into three peaks at 398.7, 400.4, and 401.3 eV. The former two peaks would be attributed to hydrogen-bonded NH_2 and hydrogen-bonded protonated amines, respectively, though they slightly shift to lower binding energies comparing with the N_{1s} XPS spectrum of $(C_{12})_{0.554}GO$. The later peak is caused by NH_3^+ groups (Fig. 10c). When the $(C_{12})_{1.780}GO$ with excess C_{12} was washed with ethanol several times, the resulting sample shows an almost identical N_{1s} XPS spectrum to $(C_{12})_{0.554}GO$ (Fig. 9): the peak is deconvoluted into two peaks at 399.6 and 400.8 eV. In addition to this change, the interlayer spacing greatly decreases from 2.64 to 1.99 nm as shown in Fig. 11. According to the literature [24], we attribute this phenomenon to the replacement of some neutral hydrogen-bonded C_{12} (Fig. 10a) by ethanol molecules which are removed from the interlayer during the washing and drying process. In order to keep equilibrium, the ionically bound C_{12} (Fig. 10c) decreases together with the regeneration of hydrogen-bonded protonated C_{12} (Fig. 10b) and increase

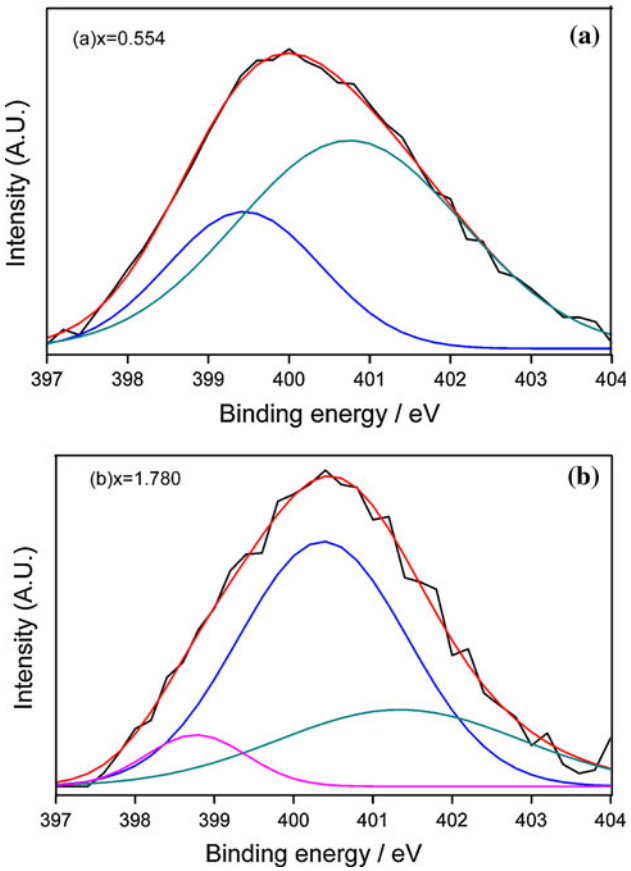

Fig. 8 XPS spectra of **a** $(C_{12})_{0.554}GO$ and **b** $(C_{12})_{1.780}GO$ in N_{1s} region

of hydrogen-bonded neutral C_{12} (Fig. 10a). Just as the titration curve has proved, there is more than one kind of exchangeable protons in the $(C_{12})_xGO$.

Characterization of reduced laurylamine-intercalated GO

As for the analysis of the reduction of the laurylamine-intercalated GO, we took the reduced $(C_{12})_{0.554}GO$ [$R(C_{12})_{0.554}GO$] and reduced $(C_{12})_{1.582}GO$ [$R(C_{12})_{1.582}GO$] as the samples, considering the different interaction

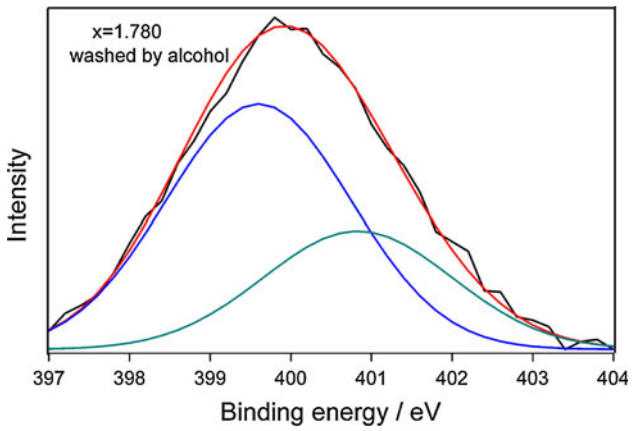

Fig. 9 XPS spectra of $(C_{12})_{1.780}GO$ washed with alcohol several times in N_{1s} region

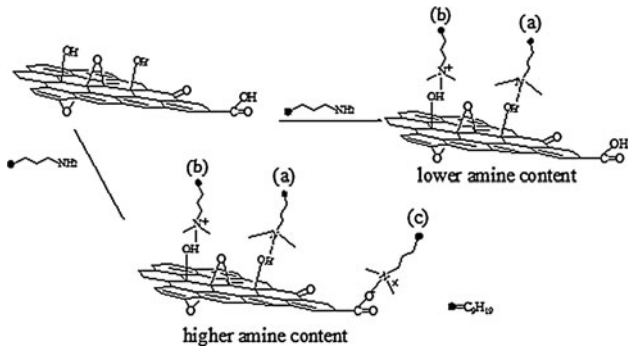

Fig. 10 Models for the interaction between C_{12} and GO: (*a*) hydrogen bonded-neutral C_{12}, (*b*) hydrogen-bonded ammonium-type C_{12}, and (*c*) ionically bonded ammonium-type C_{12}. *Dotted lines* indicate the hydrogen bonding

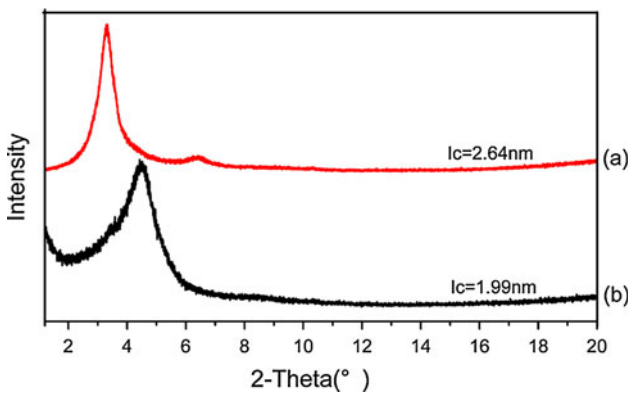

Fig. 11 X-ray diffraction patterns of $(C_{12})_{1.780}GO$ before (*a*) and after (*b*) washed by alcohol

mechanism of $(C_{12})_xGO$. Figure 12 shows the wide-angle XRD patterns of GO, C_{12}, reduced GO (RGO), $R(C_{12})_{0.554}GO$, and $R(C_{12})_{1.582}GO$. GO exhibits a broad reflection with a peak at $2\theta = 11.62°$, which is correlated to

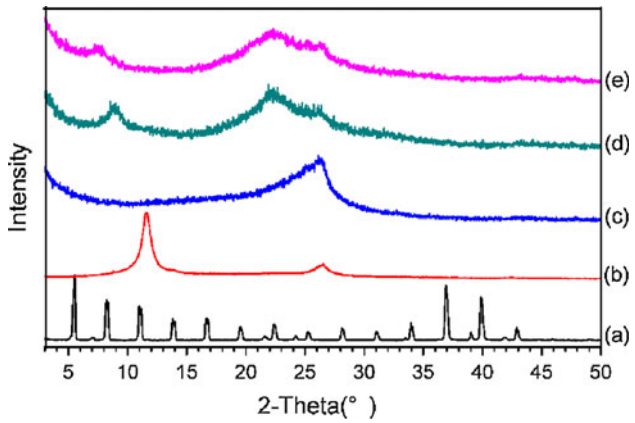

Fig. 12 Wide-angle XRD of (*a*) C_{12}, (*b*) GO, (*c*) RGO, (*d*) $R(C_{12})_{0.554}GO$, and (*e*) $R(C_{12})_{1.582}GO$

an interlayer spacing of 0.76 nm. This value can be assigned to the (001) reflection peak and might depend on the method of preparation and the amount of absorbed water in the GO [37]. The diffraction peak of graphite is also observed at $2\theta = 26.54°$, due to the partly oxidization of graphite. After GO was reduced into pure graphene, one broad reflection peak centered at $2\theta = 26.54°$ is observed in the XRD pattern of RGO, which can be correlated to an interlayer spacing of 0.34 nm in the graphene sample. The observed broad peak shows that the graphene sheets are loosely stacked in RGO [38], and it is different from the crystalline graphite. The C_{12} sample shows various reflection peaks which indicate some crystalline order of C_{12}. The peak of $(C_{12})_{0.554}GO$ at $2\theta = 3.96°$ moves to $2\theta = 8.8°$, which means the interlayer spacing changes from $d = 2.22$ to 1.0 nm after the reduction of $(C_{12})_{0.554}GO$. In the same way, the peak of $(C_{12})_{1.582}GO$ at $2\theta = 3.32°$ moves to $2\theta = 7.7°$, which means the interlayer spacing changes from $d = 2.65$ to 1.2 nm after the reduction of $(C_{12})_{1.582}GO$. This might due to the mass reduction of –C–O, –C=O, –C(O)O. Compared with RGO, the additional peaks of $R(C_{12})_{0.554}GO$ at $2\theta = 8.8°$, 22.5°, 26.1° and peaks of $R(C_{12})_{1.582}GO$ at $2\theta = 7.7°$, 22.2°, 26.2° indicate the chemical modification of graphene.

Figure 13 shows FT-IR spectra of $(C_{12})_{0.554}GO$, $R(C_{12})_{0.554}GO$, $(C_{12})_{1.582}GO$, and $R(C_{12})_{1.582}GO$. In the spectrum of $(C_{12})_{0.554}GO$, the peaks at 1080 and 1230 cm^{-1} are assigned to C–O stretching vibrations; the peak at 1372 cm^{-1} is assigned to O–H stretching vibrations. In the spectrum of $R(C_{12})_{0.554}GO$, the peak of the C–O stretching vibration can also be seen while the peak of the O–H stretching vibrations disappears. For $(C_{12})_{0.554}GO$, peaks at 1578 and 1463 cm^{-1} are due to N–H and C–H bending vibrations, respectively. As to the spectrum of $R(C_{12})_{0.554}GO$, we observe the C=C or C=N stretching vibrations at 1656 cm^{-1}, the peaks of N–H at 1564 and

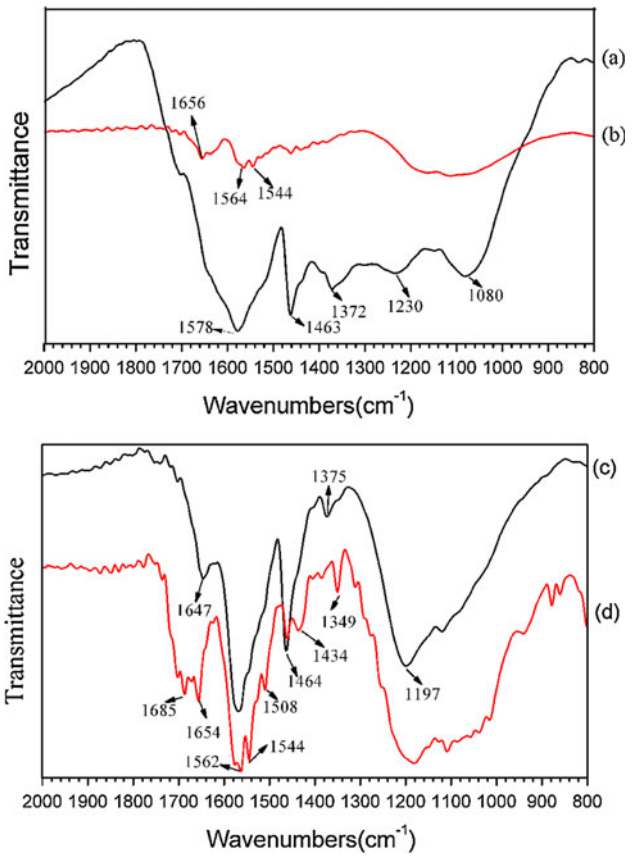

Fig. 13 IR spectra of (*a*) $(C_{12})_{0.554}GO$, (*b*) $R(C_{12})_{0.554}GO$, (*c*) $(C_{12})_{1.582}GO$, and (*d*) $R(C_{12})_{1.582}GO$

1544 cm^{-1} and the stretching vibrations of C–N around 1250–1050 cm^{-1}. In the spectrum of $(C_{12})_{1.582}GO$, the peaks at 1647 and 1562 cm^{-1} are due to N–H bending vibrations; the peaks at 1375 and 1197 cm^{-1} are assigned to C–N stretching vibrations and the peaks at 1464 cm^{-1} are due to C–H bending vibrations. As to the spectrum of $R(C_{12})_{1.582}GO$, the peaks of N–H bending vibrations at 1562, 1544, 1508 cm^{-1} and the peaks of C–N stretching vibrations at 1434 and 1349 cm^{-1} can also be seen. We also observe the peaks of C=N stretching vibrations at 1685 cm^{-1}, the peaks of C=C or C=N stretching vibrations at 1654 cm^{-1} and the peaks of C–H bending vibrations at 1654 cm^{-1}. The spectra show the existence of C–N, C=N, and N–H before and after reduction which indicate the successful preparation of C_{12}-modified graphene.

AFM characterization has been one of the most direct methods of quantifying the degree of exfoliation to graphene level after the dispersion of the powder in a solvent [39]. AFM images of $R(C_{12})_{0.554}GO$ and $R(C_{12})_{1.582}GO$ are shown in Fig. 14. Samples for AFM images were prepared by depositing dispersions of $R(C_{12})_{0.554}GO$ and $R(C_{12})_{1.582}GO$ in DMF on a freshly cleaved mica surface separately and allowed them to dry at 60 °C. The images reveal that the samples contain single-layer and double-layer sheets. The average thickness of single layer sheets is about 1.2 nm. The AFM images indicate that the modified graphene can exist in DMF in the form of single or double sheets after sonication.

Figure 15 shows the SEM images of $R(C_{12})_{0.554}GO$ and $R(C_{12})_{1.582}GO$. Commonly, the reduced GO material consists of randomly aggregated, thin-crumpled sheets closely associated with each other and forming a disordered solid [40], while the images of $R(C_{12})_{0.554}GO$ and $R(C_{12})_{1.582}GO$ show a different situation: the samples crumple at the edge of the sheets and have large surface apart from some small fragments. The image of $R(C_{12})_{0.554}GO$ is smoother than that of $R(C_{12})_{1.582}GO$ and its layered structure is more obvious, kind of similar to the structure of GO.

We also employed X-ray photoelectron spectroscopy (XPS) to analyze the samples of GO, $R(C_{12})_{0.554}GO$, and $R(C_{12})_{1.582}GO$ in C_{1s} region. In brief, the C_{1s} XPS spectrum of GO (Fig. 16a) clearly indicates a considerable degree of oxidation with four components that correspond to carbon atoms in different functional groups: the non-oxygenated ring C (284.9 eV), the C in C–O bonds (286.2 eV), the carbonyl C (C=O, 287.4 eV), and the carboxylate carbon (O–C=O) (289.2 eV) [41]. The C_{1s} XPS spectrum of the $R(C_{12})_{0.554}GO$ (Fig. 16b) also exhibits the same oxygen functionalities that have been seen in the XPS spectrum of GO, but the peak intensities of these components in the reduced samples much smaller than those in the GO, indicating considerable deoxygenation by the reduction process. In addition, there is an additional component at 285.9 eV corresponding to C bound to nitrogen [42]. The C_{1s} XPS spectrum of the $R(C_{12})_{1.582}GO$ (Fig. 16c) is similar to that of $R(C_{12})_{0.554}GO$, apart from some small shift, which means the $R(C_{12})_{1.582}GO$ has deoxygenated during the reduction process and contains the same functional groups with the $R(C_{12})_{0.554}GO$. The results conform to the FT-IR spectra analysis.

Figure 17 shows the XPS spectra of $R(C_{12})_{0.554}GO$ and $R(C_{12})_{1.582}GO$ in N_{1s} region. The $R(C_{12})_{0.554}GO$ shows an almost identical N_{1s} XPS spectrum to $(C_{12})_{0.554}GO$. The peak is deconvoluted into two peaks at 399.4 and 400.6 eV, indicating different functional groups: the hydrogen-bonded NH_2 (Fig. 10a) and hydrogen-bonded protonated amines (Fig. 10b), respectively. The $R(C_{12})_{1.582}GO$ shows an almost identical N_{1s} XPS spectrum to $(C_{12})_{1.780}GO$. The peak is deconvoluted into three peaks at 399.5, 400.3, and 401.6 eV. These peaks would be due to hydrogen-bonded NH_2 (Fig. 10a), hydrogen-bonded protonated amines (Fig. 10b), and ionically bonded ammonium (Fig. 10c), respectively. From the analysis of Fig. 17, we can see that the $R(C_{12})_{0.554}GO$ and $R(C_{12})_{1.582}GO$ are still modified by C_{12}.

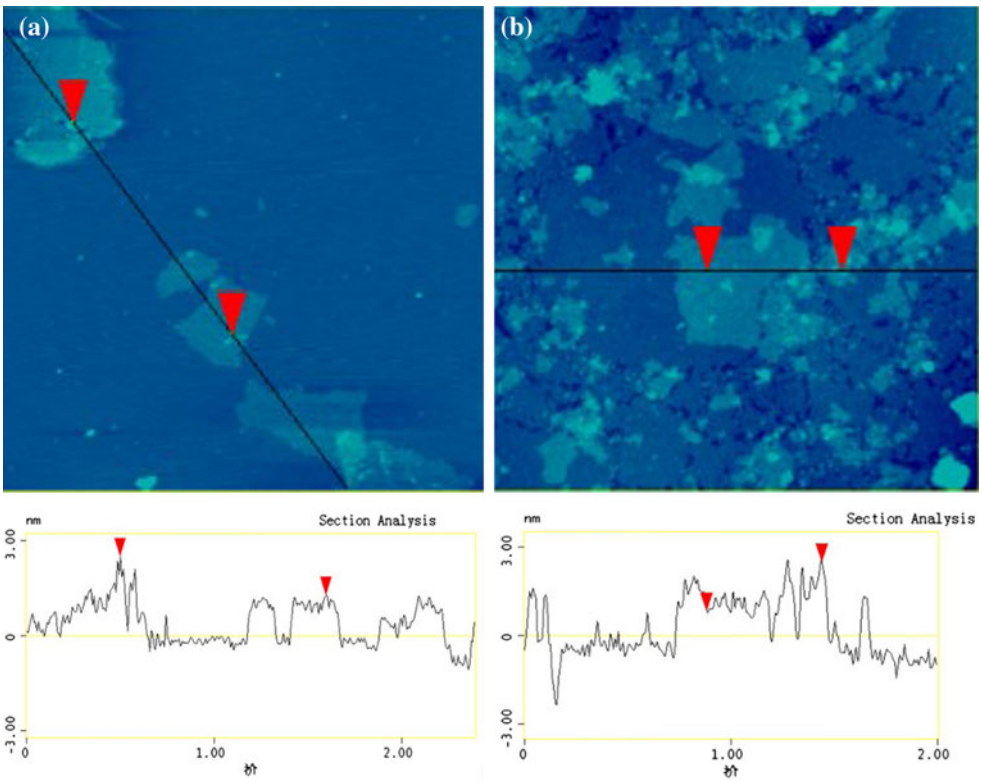

Fig. 14 AFM images of **a** $R(C_{12})_{0.554}GO$ on a mica substrate and **b** $R(C_{12})_{1.582}GO$ on a mica substrate

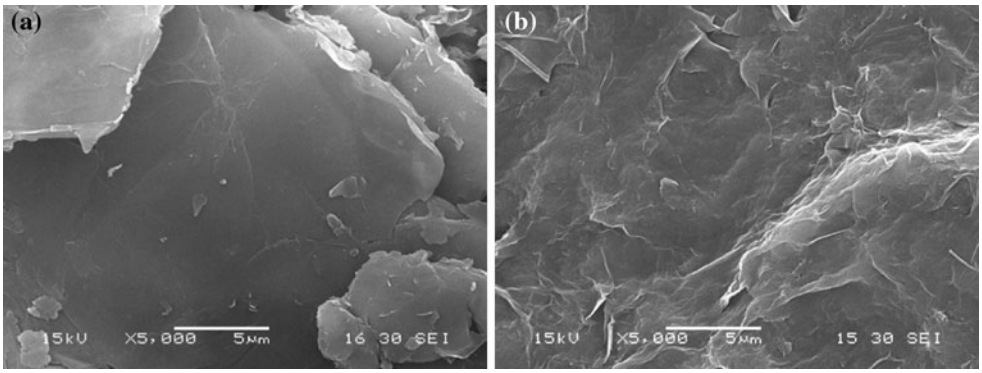

Fig. 15 SEM images of **a** $R(C_{12})_{0.554}GO$ and **b** $R(C_{12})_{1.582}GO$

Possible mechanisms for the chemical reduction of $(C_{12})_xGO$ by hydrazine

The interaction model of $(C_{12})_{0.554}GO$ and $(C_{12})_{1.582}GO$ belong to the "lower amine content" type and "higher amine content" type (Fig. 10), respectively. We have known that C_{12} exists in the form of hydrogen-bonded neutral amines and hydrogen-bonded protonated amines in the $(C_{12})_{0.554}GO$. For the $(C_{12})_{1.582}GO$, C_{12} exists in the form of hydrogen-bonded neutral amines, hydrogen-bonded protonated amines, and ionically bonded ammonium. From the XPS spectra analysis of $R(C_{12})_{0.554}GO$ in N_{1s} region (Fig. 17a), we know that C_{12} still exist in the form of hydrogen-bonded neutral amines, hydrogen-bonded protonated amines in the $R(C_{12})_{0.554}GO$. The XPS spectra analysis of $R(C_{12})_{1.582}GO$ in N_{1s} region (Fig. 17b) shows that C_{12} still exists in the form of hydrogen-bonded neutral amines, hydrogen-bonded protonated amines, and ionically bonded ammonium in the $R(C_{12})_{1.582}GO$. At present, it remains unclear as to how hydrazine reacts with GO. According to Zalan et al. [43], hydrazine is readily ring-open epoxides and forms hydrazino alcohols. One mechanistic route of the reduction of GO with hydrazine has been proposed by Stankovich et al. [40]. Stankovich thought that the formed hydrazino alcohols might react further and form a double bond. These assumptions can be applied to the chemical reduction of $(C_{12})_{0.554}GO$ and $(C_{12})_{1.582}GO$. The models for the chemical reduction of $(C_{12})_xGO$ are shown

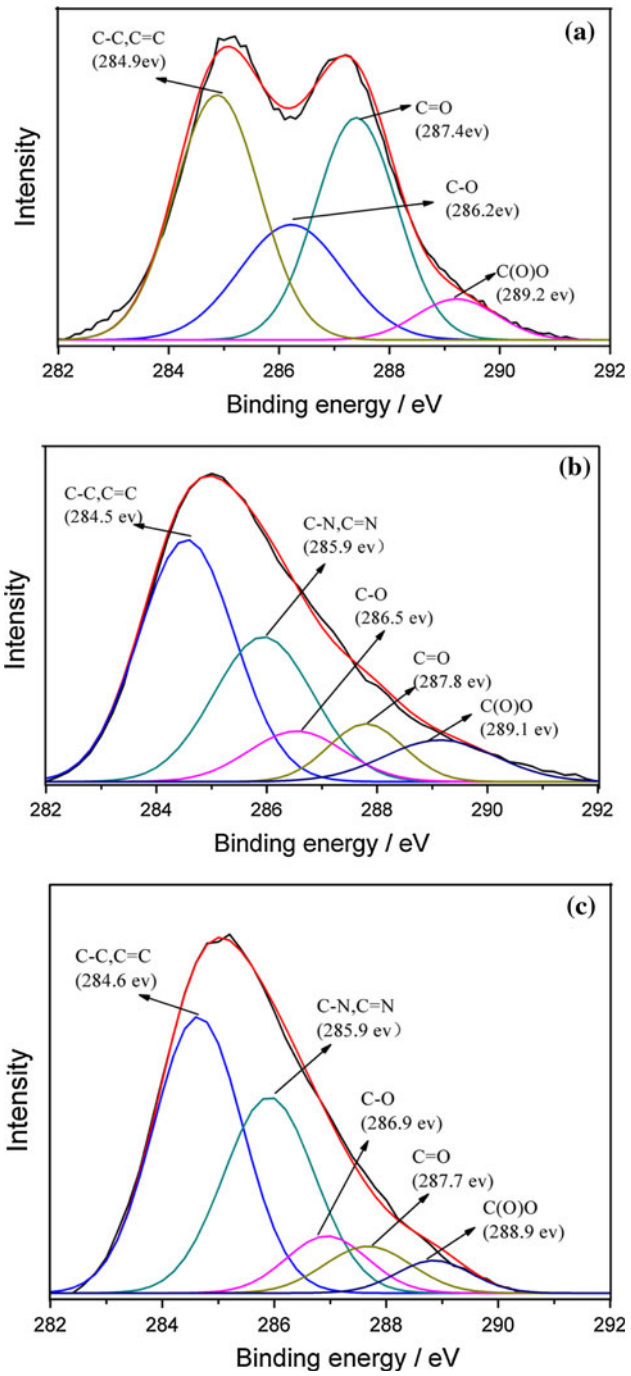

Fig. 16 XPS spectra of **a** GO, **b** $R(C_{12})_{0.554}GO$, and **c** $R(C_{12})_{1.582}GO$ in C_{1s} region

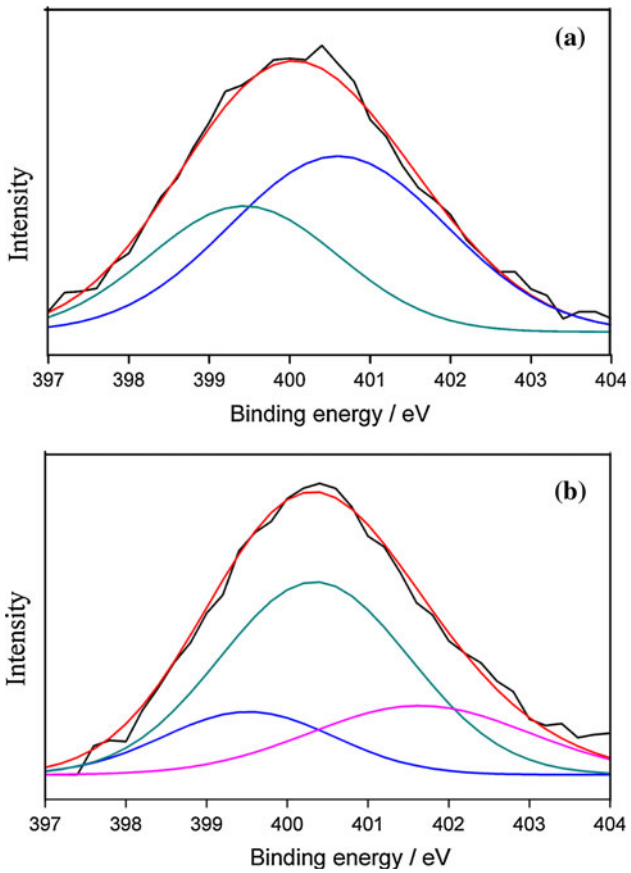

Fig. 17 XPS spectra of **a** $R(C_{12})_{0.554}GO$ and **b** $R(C_{12})_{1.582}GO$ in N_{1s} region

in Figs. 18 and 19. The hydrazine ($H_2N–NH_2$) opens the ring of epoxides, forming –OH and $HN–NH_2$. Then the further reaction between –OH and $HN–NH_2$ forms C=C in $R(C_{12})_xGO$ and $HO–NH–NH_2$. This explains the increase of C=C, which is shown in XPS (Fig. 16). In addition, there might be a reaction happens between –C=O of $(C_{12})_xGO$ and $H_2N–NH_2$, forming H_2O and $–C=N–NH_2$ which can be used to explain the incorporation of nitrogen into the $R(C_{12})_xGO$. Compared with the $(C_{12})_{1.582}GO$, the $(C_{12})_{0.554}GO$ should have an extra reaction with $H_2N–NH_2$ since the –COOH not react with C_{12} during the modification of GO. The reaction between –COOH and $H_2N–NH_2$ of $(C_{12})_{0.554}GO$ also bring nitrogen into the $R(C_{12})_{0.554}GO$. These explanations conform to the analysis of FT-IR (Fig. 13) and XPS (Fig. 16). The XPS analysis implies the quantity change of –C–O, –C=O, –C(O) O, and –C=C– in $(C_{12})_xGO$ after the chemical reduction. The decrease of –C–O, –C=O, and –C(O) O groups amount might cause the change of interlayer spacing before and after reduction, as shown in Figs. 3 and 12.

Conclusions

A detailed study on the preparation and characterization of laurylamine-intercalated GO and its reduction has been performed. The conclusions as follows: first, we present a new method of preparing laurylamine-intercalated GO. Second, the modification mechanism of GO is discussed. Three types of C_{12} in GO are identified in the obtained intercalation compounds: hydrogen-bonded neutral amines,

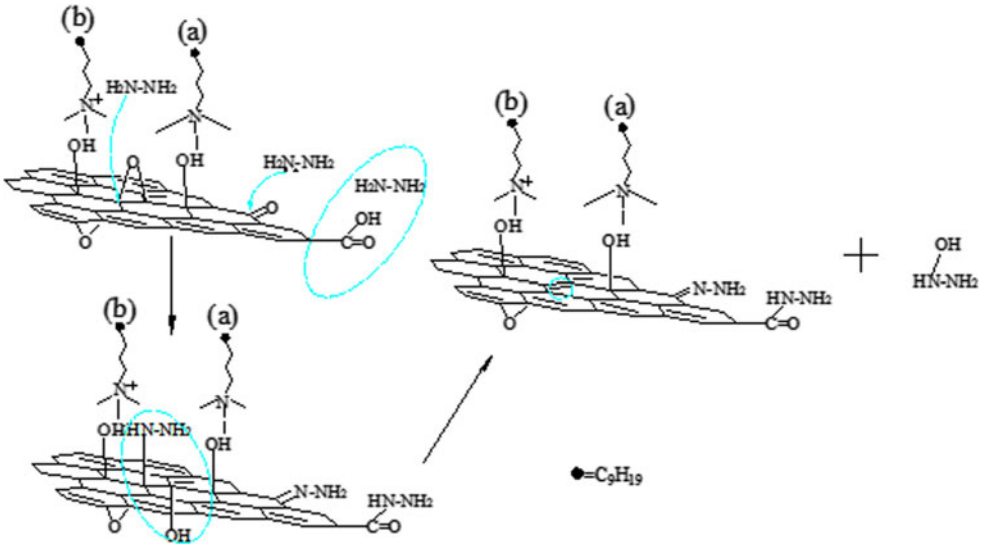

Fig. 18 Models for the reduction of $(C_{12})_{0.554}GO$

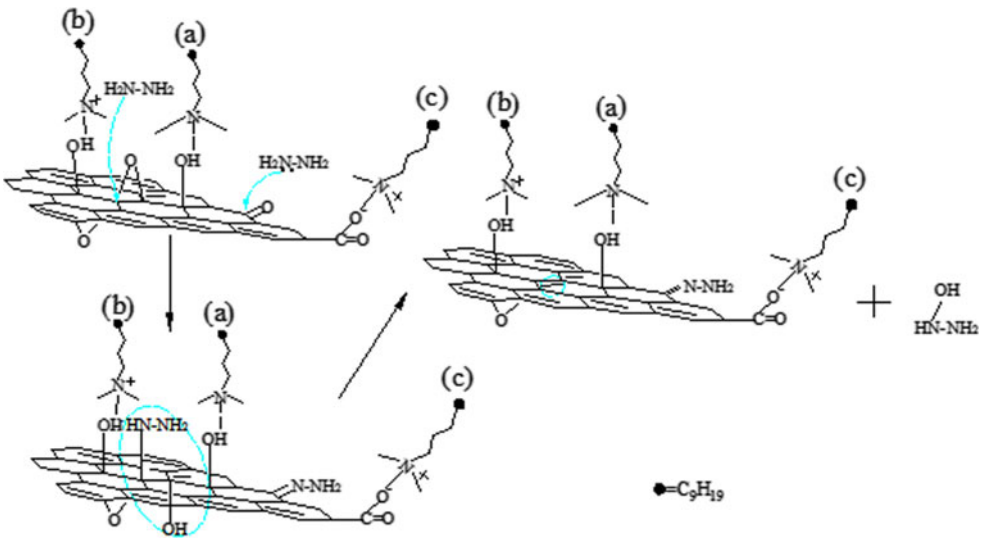

Fig. 19 Models for the reduction of $(C_{12})_{1.582}GO$

hydrogen-bonded protonated amines, and ionically bound protonated amines. The former two types are observed in the "lower amine content" $(C_{12})_xGO$ ($x \leq 0.672$), while the "higher amine content" $(C_{12})_xGO$ ($x \geq 0.791$) has these three types. In addition, stable colloidal suspensions of modified graphene in DMF are prepared by the chemical reduction of hydrazine. Based on the XRD, FT-IR, and XPS studies, we put forward the possible reduction mechanism. Compared with the "higher amine content" $(C_{12})_xGO$, the "lower amine content" $(C_{12})_xGO$ has an extra reaction with $H_2N–NH_2$ during the reduction process. The types of C_{12} existed in $R(C_{12})_xGO$ is the same as the way of C_{12} exists in $(C_{12})_xGO$. The reached colloidal suspensions are of great importance in the preparation of many types of materials, including composites, fibers, and thin film materials, and the suspensions of modified graphene hold great promise in this regard.

Acknowledgements The authors are grateful for the financial support from the 863 program. The program No. is 2009AA04Z142.

References

1. Lerf A, He H, Forster M, Klinowski J (1998) J Phys Chem 102: 4477
2. He H, Riedl T, Lerf A, Klinowski J (1996) J Phys Chem 100: 19954
3. Chen XG, He YQ, Zhang Q, Li LJ, Hu DH, Yin T (2010) J Mater Sci 45:953. doi:10.1007/s10853-009-4025-3
4. Matsuo Y, Tahara K, Sugie Y (1996) Carbon 34:672
5. Matsuo Y, Tahara K, Sugie Y (1997) Carbon 35:113
6. Dékány I, Kruger-Grasser R, Weiss A (1988) Colloid Polym Sci 276:570
7. Matsuo Y, Fukutsuka T, Sugie Y (2002) Carbon 40:958
8. Matsuo Y, Fukunaga T, Tokura N, Fukutsuka T, Sugie Y (2004) Trans Mater Res Soc Jpn 29:3219
9. Liu Y, Chen ZM, Yang GS (2010) J Mater Sci. doi:10.1007/s10853-010-4829-1

10. Matsuo Y, Hatase K, Sugie Y (1999) Chem Lett 10:1109
11. Matsuo Y, Fukutsuka T, Sugie Y (2003) Chem Lett 32:1004
12. Yazamia R, Touzain Ph, Chouteau G, Briggs A (1985) Synth Met 12:485
13. Stoller MD, Park SJ, Zhu YW, An J, Ruoff RS (2008) Nano Lett 8:3498
14. Dikin DA, Stankovich S, Zimney EJ, Piner RD, Dommett GHB, Evmenenko G, Nguyen ST, Ruoff RS (2007) Nature 448:457
15. Stankovich S, Dikin DA, Dommett GHB, Kohlhaas KM, Zimney EJ, Stach EA, Piner RD, Nguyen ST, Ruoff RS (2006) Nature 442:282
16. Ji ZY, Wu JL, Shen XP, Zhou H, Xi HT (2010) J Mater Sci. doi: 10.1007/s10853-010-4892-7
17. Bunch JS, van der Zande AM, Verbridge SS, Tanenbaum DM, Parpia JM, Craighead HG, McEuen PL (2007) Science 315:490
18. Ni ZH, Wang HM, Kasim J, Fan HM, Yu T, Wu YH, Feng YP, Shen ZX (2007) Nano Lett 7(9):2758
19. Lomeda JR, Doyle CD, Kosynkin DV, Hwang WF, Tour JM (2008) J Am Chem Soc 130(48):16201
20. Park SJ, An J, Piner RD, Jung I, Yang DX, Velamakanni A, Nguyen ST, Ruoff RS (2008) Chem Mater 20(21):6592
21. Ferralis N (2010) J Mater Sci 45:5135. doi:10.1007/s10853-010-4673-3
22. Stankovich S, Piner RD, Chen XQ, Wu NQ, Nguyen ST, Ruoff RS (2006) J Mater Chem 16:155
23. Bourlinos AB, Gournis D, Petridis D, Szabó T, Szeri A, Dékány I (2003) Langmuir 19:6050
24. Matsuo Y, Miyabe T, Fukutsuka T, Sugie Y (2007) Carbon 45: 1005
25. Nethravathi C, Rajamathi M (2006) Carbon 44:2635
26. Hummers WS, Offeman RE (1958) J Am Chem Soc 80:1339
27. Matsuo Y, Watanabe K, Fukutsuka T, Sugie Y (2003) Carbon 41:1545
28. Dreyer DR, Park SJ, Bielawski CW, Ruoff RS (2010) Chem Soc Rev 39:228
29. McAllister MJ, Li JL, Adamson DH, Schniepp HC, Abdala AA, Liu J, Alonso MH, Milius DL, Car R, Prud'homme RK, Aksay IA (2007) Chem Mater 19:4396
30. Higginbotham AL, Kosynkin DV, Sinitskii A, Sun ZZ, Tour JM (2010) ACS Nano 4(4):2059
31. Hahn JR, Kang H, Lee SM, Lee YH (1999) J Phys Chem B 103:9944
32. Cassagneau T, Guerin F, Fendler JH (2000) Langmuir 16(18): 7318
33. Szabó T, Tombácz E, Illés E, Dékány I (2006) Carbon 44:537
34. Szabo T, Berkesi O, Forgo P, Josepovits K, Sanakis Y, Petridis D (2006) Chem Mater 18:2740
35. Chernyshova IV, Rao KH, Vidyadhar A, Shchukarev AV (2000) Langmuir 16:8071
36. Matsuo Y, Tabata T, Fukunaga T, Fukutsuka T (2005) Carbon 43:2875
37. Liu ZH, Wang ZM, Yang XJ, Ooi K (2002) Langmuir 18:4926
38. Zhang K, Zhang LL, Zhao XS, Wu JS (2010) Chem Mater 22(4):1392
39. Shen JF, Hu YZ, Shi M, Lu X, Qin C, Li C, Ye MX (2009) Chem Mater 21:3514
40. Stankovich S, Dikin DA, Piner RD, Kohlhaas KA, Kleinhammes A, Jia YY, Wu Y, Nguyen ST, Ruoff RS (2007) Carbon 45:1558
41. Briggs D, Beamson G (1992) High resolution XPS of organic polymers: the scienta ESCA300 database. John Wiley and Sons, New York
42. Waltman RJ, Pacansky J, Bates CW Jr (1993) Chem Mater 5:1799
43. Zalan Z, Lazar L, Fueloep F (2005) Curr Org Chem 9:357